Assessment of 21 years of Arctic Ocean Absolute Sea Level Trends (1995-2015)

Carsten Ankjær Ludwigsen[1], Ole Baltazar Andersen[1], and Stine Kildegaard Rose[1]

[1]DTU Space, Elektrovej 328, 2800 Kgs. Lyngby, Denmark

Correspondence: Carsten Ankjær Ludwigsen (caanlu@space.dtu.dk)

Abstract. The Arctic Ocean is at the frontier of the fast changing climate in the northern latitudes. As the first study, we validate and assess the components of the observed sea level trend from altimetry and tide gauges (TG), without using observations from the Gravity Recovery and Climate Experiment (GRACE). This approach permits a longer time series and avoids problems with errors from leakage effects associated with GRACE. Steric and manometric sea level change is reconstructed and is combined into an Arctic sea level estimate, that is independent from any observed sea level change. Relative sea level observed by 12 selected tide gauges is corrected with novel vertical land movement (VLM) estimates accounting for past and contemporary deglaciation. The calculations shows that contemporary deglaciation alters the Arctic absolute sea level of around 1 mm y^{-1}, while salinity-driven halosteric sea level trend is dominating the sea level trend with variations between -7 and 10 mm y^{-1}.

Large uncertainties originate from limited data to constrain the steric data in some regions of the Arctic while also altimetry is visibly challenged in sea ice covered areas. The reconstructed sea level estimate agrees (within uncertainty) with the observed sea level from altimetry in 98% of the Arctic and for 11 of 12 TGs. The correlation between the reconstructed estimate and altimetry (R=0.50) clearly outperforms a similar study using GRACE-estimates. The results confirm a large negative absolute sea level trend shown by other studies in the eastern Siberian Arctic, that is in contrast to the significant sea level rise observed in the area by TGs.

1 Introduction

The Arctic is globally the region with the fastest changing climate and is warming twice the rate of the global average (Box et al., 2019). The resulting enhanced deglaciation of land, sea ice cover decrease and ocean freshening has several affects on sea level, hence understanding sea level in the Arctic Ocean paramount for mapping consequences of climate change. At the same time, oceanographic in-situ observations and satellite observations of the Arctic are prone to challenges from an harsh environment, sea ice floats and lack of spatial coverage (Smith et al., 2019).

Satellite altimetry has been measuring the Arctic Ocean since 1991 with ESA's European Remote Sensing (ERS)-1 satellite being the first reaching polar latitudes. (Laxon et al., 2003) were the first to study Arctic sea level from the ERS-1/2 satellites to produce sea-ice thicknesses. Since then many have followed e.g. (Peacock and Laxon, 2004; Prandi et al., 2012; Cheng et al., 2015; Rose et al., 2019), but uncertainties in particular in sea ice-covered regions are still present (Armitage et al., 2016; Rose et al., 2019; Raj et al., 2020).

Reconstructing sea level change with the sea level budget is useful both to constrain sea level observations and separate steric-driven and manometric sea level change (Gregory et al., 2019) and hence quantify the origins of sea level change. The sea level budget has been assessed on global and basin-wide scales since the 19th century by using a combination of in-situ data, satellite observations and probabilistic analysis (Church and White, 2011a; WCRP, 2018; Dangendorf et al., 2019; Royston et al., 2020; Frederikse et al., 2020), but these studies tends to neglect the polar region.

Previous attempts to reconstruct sea level in the Arctic has shown to be difficult (Henry et al., 2012; Armitage et al., 2016; Carret et al., 2017; Ludwigsen and Andersen, 2020; Raj et al., 2020), because both satellite observations and in-situ observations are less consistent than in low and mid-latitudes. Observations from the Gravity Recovery And Climate Experiment (GRACE) offer the only direct Arctic-wide measurements of manometric sea level change since mid-2002. However, discrepancies of over 10 mm y^{-1} (Ludwigsen and Andersen, 2020) exist among different GRACE-products (Wiese et al., 2016; Save et al., 2016; Luthcke et al., 2013), and previous studies often tend to choose the solution that has the best agreement with the absolute sea level observed by altimetry and modeled steric sea level (Carret et al., 2017; Raj et al., 2020).

In this paper, we attempt to assess the satellite and tide gauge observed Arctic sea level trends from 1995-2015 by reconstructing the sea level response to contemporary land ice loss, glacial isostatic adjusment (GIA) and atmospheric pressure (inverse barometer, IB) and thereby mapping the long-term manometric sea level change without GRACE. The time series of 21 years is generally 8 years more than assessments using GRACE (Armitage et al., 2016; Carret et al., 2017; Raj et al., 2020). This has the advantage, that non-secular and inter-annual dynamic effects, which are mainly driven by the Arctic Oscillation, (Henry et al., 2012; Armitage et al., 2018) are reduced.

2 Method

Sea level observations from satellite altimetry are measured relative to a terrestrial reference frame and is called geocentric or absolute sea level (ASL). Tide gauges (TG) measures the sea level while being grounded to the coast, and is affected by vertical land movement (VLM). The ASL (similar to altimetry) can be reconstructed by adding vertical land movement (VLM), defined with respect to the same reference frame as altimetry, to tide gauge-measured relative sea level (RSL).

$$\mathrm{ASL} = \mathrm{RSL} + \mathrm{VLM} \tag{1}$$

Changes of ASL ($\dot{\mathrm{ASL}}$) originates either from changed ocean density (steric, $\dot{\eta}$) due to changes in salinity (halosteric) or temperature (thermosteric) or from changes in ocean mass, which is defined as manometric sea-level change, $\dot{\mathrm{M}}$ (Gregory et al., 2019)). According to (Gregory et al., 2019), manometric sea level change can be referred to as the 'non-steric' sea level change and is indifferent to the commonly used Ocean Bottom Pressure (OBP).

$$\dot{\mathrm{ASL}} = \dot{\eta} + \dot{\mathrm{M}} \tag{2}$$

As already mentioned, the steric sea level change can be split into halosteric ($\dot{\eta_S}$) and thermosteric ($\dot{\eta_T}$) sea level change:

$$\dot{\eta} = \dot{\eta}_S + \dot{\eta}_T \tag{3}$$

The manometric component is further divided into contributions from changes in the gravitational field, G that together with a spatial uniform constant, c, composes the gravitational sea level fingerprint (N) due to different land-to-ocean mass changes, i, which in this study originates from either different sources of land ice (Greenland (GRE), Northern Hemisphere (NH) Glaciers and Antarctica (Ant) + Southern Hemisphere (SH) glaciers) or GIA. Change in IB is also part of the total manometric sea level change, $\dot{\mathrm{M}}$.

$$\dot{\mathrm{M}} = \sum_i \dot{N}_i + \dot{\mathrm{IB}} \quad \text{, where} \quad \dot{N}_i = \dot{G}_i + \dot{c}_i \tag{4}$$

VLM is split into the viscoelastic solid earth deformation caused from past millennial ice (un-)loading, GIA, and the elastic adjustment from contemporary (1995-2015) change in ice loading, VLMe, which, as G, is a composite of the elastic response from different origins of land ice (i).

$$\dot{\mathrm{VLM}} = \dot{\mathrm{GIA}} + \sum \dot{\mathrm{VLMe}}_i \tag{5}$$

By substituting eq. 4 and eq. 3 into eq. 2, we achieve the reconstruction of absolute sea level, ASL_r, that is comparable with the observed ASL by satellite altimetry (denoted as $\mathrm{ASL_A}$):

$$\dot{\mathrm{ASL}}_r = \sum(\dot{G}_i + \dot{c}_i) + \dot{\mathrm{IB}} + \dot{\eta}_S + \dot{\eta}_T \tag{6}$$

Thirdly, a TG-based ASL estimate, $\mathrm{ASL_{TG}}$, is achieved by adding eq. 5 to eq. 1:

$$\dot{\mathrm{ASL}}_{\mathrm{TG}} = \dot{\mathrm{RSL}}_{\mathrm{TG}} + \mathrm{GIA} + \sum \dot{\mathrm{VLMe}}_i \tag{7}$$

3 Data

This study combines various in-situ data (temperature and salinity (T/S) profiles and TG-data), satellite (GRACE and altimetry) and model data (VLM-model and ECCOv4r4) to reconstruct the Arctic sea level change. In this section follows a description of the different datasets and how they are obtained.

3.1 Altimetry

The DTU/TUM Arctic Ocean Sea Level Anomaly (SLA) record (Rose et al., 2019) provides an independent estimate of ASL change ($\mathrm{ASL_A}$). The altimetric time series is covering the whole altimetric era given as monthly grids from September 1991 to September 2018, covering 65° N to 81.5°N and 180°W–179.5°E.

The product is corrected by geophysical corrections such as tides and atmospheric delays. Leads (cracks in the sea ice cover) and open ocean are located and separated according to the different classification of their surfaces. The detection of leads is not flawless, and their sparse distribution in the sea ice cover, and the uncertainty of the the applied geophysical corrections in the Arctic (Stammer et al., 2014; Ricker et al., 2016) makes the sea level estimates more uncertain in the sea ice covered region.

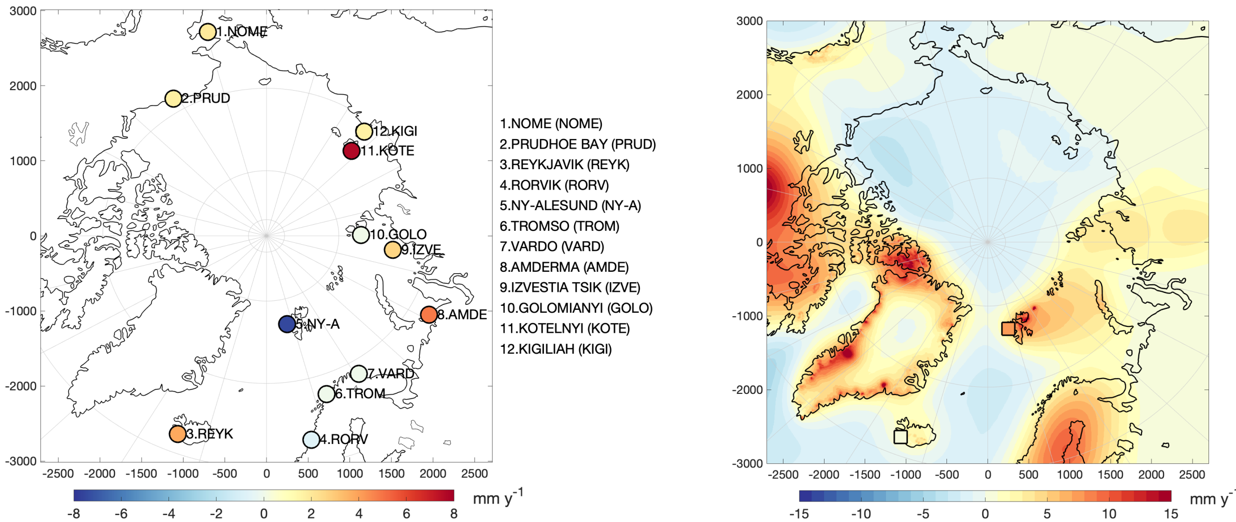

Figure 1. Left: 1995-2015 RSL trend [mm y^{-1}] and location of the selected tide gauges of this study. Right: 1995-2015 VLM-trend [mm y^{-1}] from the model of Ludwigsen et al. (2020b). The VLM-trend from the GNSS-sites at Reykjavik and Ny-Ålesund are shown with squared color coded markers.

The altimetric record includes data from four ESA satellites: ERS-1 (1991-1995), ERS-2 (1995-2003), Envisat (2002-2010) and CryoSat-2 (2010-2018). It combines results of different retrackers as well as conventional and SAR-altimetry, which may lead to biases (Rose et al., 2019). In particular ERS-1/2 has a relatively low spatial resolution and thereby limiting the measurements from leads in sea ice, while the SAR altimeter on CryoSat-2 is made to measure over the sea ice cover, which decreases the uncertainty (Rose et al., 2019). The applied version of the DTU/TUM altimetry product is not corrected for atmosphere pressure loading to be able to compare to the tide gauges. The altimetric sea level trend is shown in the results section (the middle panel of figure 5).

3.2 Tide Gauges and Vertical Land Movement

TG-data is obtained from the Permanent Service of Sea Level (PSMSL)-database (Holgate et al., 2012) given as monthly SLA. TGs with a consistent time series are few and unevenly distributed in the Arctic (Henry et al., 2012; Limkilde Svendsen et al., 2016). Usually, TG-observed RSL is aligned to ASL by utilizing vertical velocities from a nearby Global Navigation Satellite System (GNSS) receiver. Restricting TGs to locations with usable GNSS significantly limits the selection further. Therefore, an Arctic-wide VLM-model (Ludwigsen et al., 2020a) as a substitute for GNSS is applied (figure 1).

The VLM-model is composed from eq. 5. The GIA-component is based on the Caron2018 GIA-model (Caron et al., 2018), which includes an uncertainty estimate. Reported discrepancies from other GIA-models in central North America and Greenland (Caron et al., 2018; Ludwigsen et al., 2020a) has little affect at the locations of TGs of this study. Annual rates of VLMe is estimated from the 1995-2015 annual change of land ice using the Regional Elastic Rebound Calculator (REAR) (Melini et al., 2015). REAR also provides the gravitational response G to land ice change used for estimating the manometric sea level. Uncertainties of the elastic VLM-estimates are mainly due to uncertainties of the applied land ice change. An additional 10% of the VLM-signal (after Wang et al. (2012)) is added to represent uncertainties associated with the REF6371 Earth model (Kustowski et al., 2007) applied in REAR. The VLM contribution from non-tidal ocean loading (NOL) (van Dam et al., 2012) and rotational feedback (RF) (King et al., 2012) are in total of an order of ± 0.3 mm y^{-1} and are included in the VLM-contribution from Northern Hemisphere glaciers.

12 TGs are selected (geographical locations shown in figure 1) based on visual inspection of the monthly time series and to ensure that as many regions of the Arctic is represented as possible. 3-month averaged time series and linear trend of TG observed sea level (RSL_{TG}) and VLM-corrected sea level (ASL_{TG}) from 1995-2015 is shown in figure 2. The annual VLM-model is interpolated onto the TG time series and the linear trend is determined with least-squares method using months with available data between 1995 and 2015. In particular, the Alaskian and Siberian TGs have months with no or unreliable data (flagged by PSMSL). However, there is no evident seasonality in the missing months and therefore does not significantly affect the trend-estimates with a seasonal bias.

Ny-Ålesund and Reykjavik TG experience extraordinary VLM that is caused by substantial deglaciation during the Little Ice Age (LIA) (Svalbard) and low mantle viscosities in Iceland and Greenland. This is not captured in the spatially uniform REF6371 earth model. Therefore, the two sites are corrected with nearby GNSS (Global Navigation Satellite System) instead of the VLM-model. GNSS is uncertain at Prudhoe Bay, where it measures a significant subsidence, that is considerably different from the VLM-model. This is likely caused by near-by construction or oil depletion sites. However, the tide gauge is located on a peninsula reaching into the Beaufort Sea 10 km away from the GNSS-location, which is why the VLM-model is trusted over the GNSS-measurement.

Reykjavik (64.2°N), Nome (64.5°N), and Rorvik (64.9°N) are located off the edge of the altimetric data, which only extends to 65°N, but are nevertheless included to extend the spatial distribution of the TG-sites.

From figure 2, we see that the RSL-trends in the Arctic vary with nearly +/- 1 cm y^{-1}, with Ny-Ålesund on Svalbard having a negative RSL-trend of -7.45 mm y^{-1}, while Kostelnyi Island between the Laptev and East Siberian Sea shows a positive trend of 7.67 mm y^{-1}. However, after applying the VLM-correction, does all TGs show a positive ASL-trend within a range of 0.3 mm $^{-1}$ (Prudhoe Bay) and 6.5 mm $^{-1}$ (Kostelnyi).

3.3 Steric sea level

The DTU steric sea level change is computed as described in Ludwigsen and Andersen (2020). The steric sea level change is computed from a three dimensional T/S-grid that is interpolated from a over 300.000 T/S profiles and thus not constrained by any satellite observations. The independent steric sea level estimate is in contrast to Morison et al. (2012) and Armitage and Davidson (2014), that use a difference between altimetry and GRACE to estimate steric heights.

T/S-profiles from buoys, ice-tethered profiles and ship expeditions in the Arctic Ocean are spatial and temporal unevenly distributed and also depends on seasonal accessibility (Behrendt et al., 2017). Especially, the data density is poor in the shallow

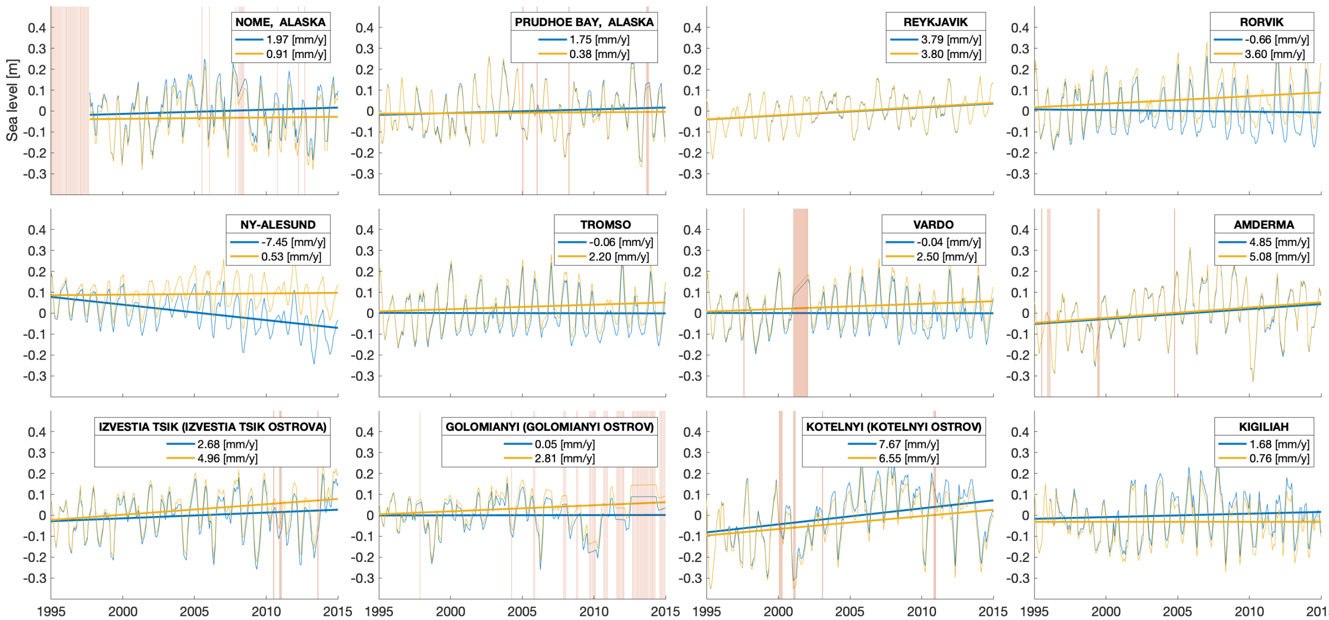

Figure 2. Relative sea level [m] from 1995-2015 registered at the 12 tide gauge from the PSMSL-database (Holgate et al., 2012)]. Blue line represents the 3-month running average, while the thick line is the linear trend (trend estimate [mm y^{-1}] shown in legend). Yellow line represents the absolute sea level and trend, equal to the blue line corrected for VLM with a VLM-model (Ludwigsen et al., 2020b) (except Ny-Ålesund and Reykjavik that are corrected with GNSS). The vertical lines indicate where observations are missing and the sea level is linearly interpolated from adjacent months.

seas along the Siberian Coast (Ludwigsen and Andersen, 2020), which is cause to large uncertainties. Temperature and salinity data are interpolated by kriging into a monthly 50x50 km spatial grid on 41 depth levels. If values are more than 3σ away from the mean of neighbouring grid cells, values from the same month in adjacent years is used.

Following the notion of Gill and Niller (1973); Stammer (1997); Calafat et al. (2012); Ludwigsen and Andersen (2020), the change in steric sea level is calculated as the sum of halosteric sea level, η_S and thermosteric sea level, η_T (equation 3). From the depth profiles of the temperature and salinity grid, η_S and η_T are calculated:

$$\eta_S = -\frac{1}{\rho_0}\int_{-H}^{0} \beta S' dz \tag{8}$$

$$\eta_T = \frac{1}{\rho_0}\int_{-H}^{0} \alpha T' dz \tag{9}$$

where H denotes the minimum height (maximum depth (z)). S' and T' are defining salinity and temperature anomalies, with reference values (as used in Ludwigsen and Andersen (2020)) are 0 C°and 35psu, respectively. β is the saline contraction coefficient and α is the thermal expansion coefficient. The opposite sign of η_S is needed since β represents a contraction

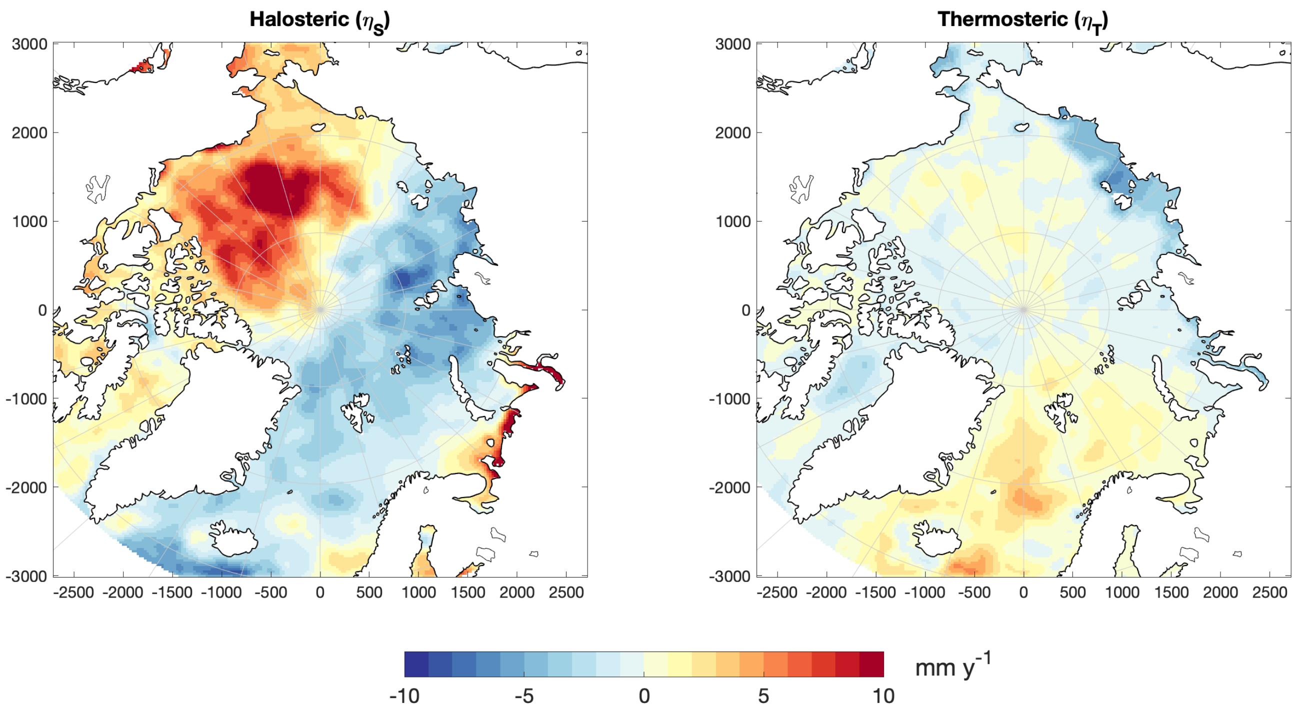

Figure 3. Halo- and thermosteric sea level trend [mm y^{-1}] from 1995-2015 derived from the DTU Steric sea level product used in Ludwigsen and Andersen (2020).

(opposite to thermal expansion). α and β are functions of absolute salinity, conservative temperature and pressure, and is determined with help from the freely available TEOS-10 software (Roquet et al., 2015). Sea level trends of η_S and η_T from 1995-2015 are shown in figure 3.

3.4 Manometric sea level contributions

Maps of the individual contributions (from equation 4) to changes in manometric sea level are shown in figure 4. The gravitational change ($\dot{G}$) of contemporary changes in ice loading (equation 4) is (similar to the elastic VLM-component) computed using the elastic greens functions by REAR (Melini et al., 2015). The gravitational change from GIA is derived from the Caron2018-model. The sea level fingerprint (figure 4a-d) is retrieved by adding the spatially invariant constant c (barystatic sea level change) to the gravitational change and is equal to the contribution to global mean sea level (Spada, 2017). Following Spada (2017), c is defined as

$$c_i = -\frac{M_i \rho_w}{A_O} - \left\langle G_i - \mathrm{VLM}_i \right\rangle \tag{10}$$

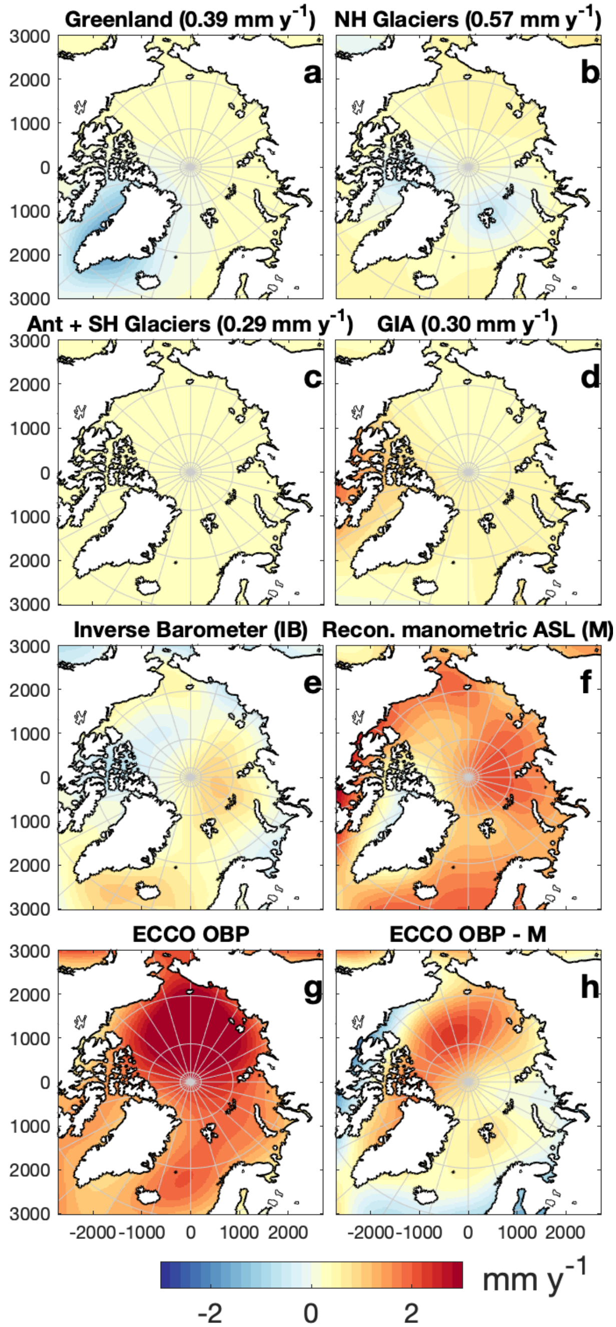

Figure 4. Contributions to the Arctic manometric sea level trend [mm y^{-1}] from 1995-2015. a-d shows $\dot{N}$ (eq. 4) for different sources of land-to-ocean mass changes with the barystatic sea level contribution ($\dot{c}$) written in brackets: Greenland (incl. pherical glaciers) (a), Northern Hemisphere (NH) glaciers (b), Antarctica (Ant) + Southern Hemisphere (SH) glaciers (c), and GIA (d). The estimated Inverse Barometer trend (e). The sum of a-e and hence the total reconstructed manometric sea level trend (f). Modelled OBP-estimate from ECCOv4r4 (Fukumori et al., 2019) (g). Difference between g and f (h).

, where M_i is the mass change of the ice model, A_O is the total ocean area, ρ_w is the average density of ocean water and $\langle ... \rangle$, denotes the average of the ocean surface. For calculating c_i, G_i and VLM_i for glaciers with REAR, individual glacial mass estimates are combined into a high resolution model for ice height change (Marzeion et al., 2012; Ludwigsen et al., 2020a). These estimated are combined with ice models for Greenland (Khan et al., 2016) and Antarctica (Schröder et al., 2019). From 1995 to 2015, the estimated ice loss is 142 Gt y^{-1} for Greenland, 206 Gt y^{-1} for Northern Hemisphere glaciers and 105 Gt y^{-1} for Antarctica and Southern Hemisphere glaciers, consistent with recent studies by Zemp et al. (2019); Shepherd et al. (2018, 2020).

The contemporary change in ice mass, M_i, is zero for GIA, hence the barystatic GIA contribution defined from the right part of equation 10. c for GIA is 0.3 mm y^{-1} consistent with other studies (Peltier, 2009; Spada, 2017). The gravitational change of RF and NOL (<0.05 mm y^{-1}) are included in the Northern Hemisphere glacial contribution to G.

The manometric sea level change is completed with the loading from atmospheric pressure, IB (figure 4e). IB is estimated by the simple relationship derived from the hydro-static equation (Naeije et al., 2000; Pugh and Woodworth, 2014). Monthly averaged pressure estimates from National Center for Environmental Prediction (NCEP) are used for surface pressure change Δp:

$$\text{IB} = -9.948 \text{ [mm/mbar] } \Delta p \tag{11}$$

The total manometric sea level change ($\dot{\text{M}}$, figure 4f) is reconstructed as:

$$\dot{\text{M}} = \dot{N}_{\text{NHG}} + \dot{N}_{\text{GRE}} + \dot{N}_{\text{SH}} + \dot{N}_{\text{GIA}} + \dot{\text{IB}} \tag{12}$$

Figure 4g shows the OBP-trend from the ECCOv4r4-model (Estimating the Circulation and Climate of the Ocean (ECCO) version 4 release 4) (Forget et al., 2015; Fukumori et al., 2019), which is a model estimate of $\dot{\text{M}}$. The difference between ECCO and $\dot{\text{M}}$ is displayed in 4h.

4 Results

Generally, the steric (in particular the halosteric) sea level trend is dominating the spatial variability of the reconstructed sea level trend (ASL_r), with over 10 mm y^{-1} in the Beaufort Gyre and -7 mm y^{-1} in the Russian Arctic (figure 3).

In contrast, is the reconstructed manometric sea level trend ($\dot{M}$) varying between 0 and 2 mm y^{-1}, with smaller spatial variability. This is in alignment with the 2003-2015 OBP-estimates from GRACE JPL mascons (Wiese et al., 2016) used in Ludwigsen and Andersen (2020), but way smaller than the estimates from GSFC mascons (Luthcke et al., 2013) used by Raj et al. (2020) and CSR (Save et al., 2016) used by Carret et al. (2017).

Figure 4a-c shows that the contributions from contemporary ice loading has a (compared to steric) small contribution to spatial sea level variability, but the sea level fingerprints from deglaciation of Greenland and glaciers are however til clearly visible with a absolute sea level fall of 0.5 to 1 mm y^{-1}, which seems to be in agreement with global sea level fingerprint studies of Bamber and Riva (2010); Spada (2017); Frederikse et al. (2018). In total, the three figures sums to a sea level rise of around 1 mm y^{-1} in most of the Arctic, except close to areas with deglaciation (like Greenland and Svalbard).

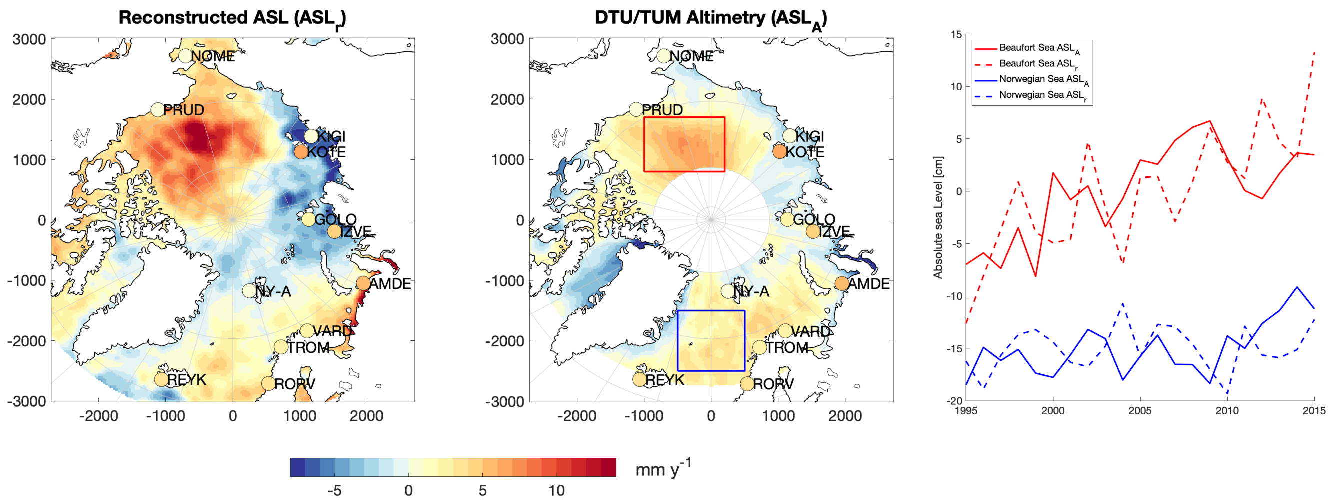

Figure 5. Absolute sea level trend of the reconstructed product ($\dot{\text{ASL}}_\text{r}$) (left) and from DTU/TUM Altimetry ($\dot{\text{ASL}}_\text{A}$) (middle) from 1995 to 2015 [mm y^{-1}]. The circles show the sea level trend of the 12 VLM-corrected tide gauges ($\dot{\text{ASL}}_\text{TG}$). Right plot shows timeseries of ASL$_\text{A}$ and ASL$_r$ for two selected areas (marked in the DTU/TUM Altimetry map).

Figure 4g shows that ECCO has a higher manometric sea level change in the interior of the Arctic Ocean, while the coastal zones, except east Siberia, are lower than $\dot{\text{M}}$.

The ECCO-model does attempt to include term dynamic sea level changes associated with wind-forcing and ocean currents into their OBP-estimate (Forget et al., 2015). Those changes are not part of $\dot{\text{M}}$ and is probably the main reason for the difference between ECCO OPB and $\dot{\text{M}}$.

4.1 Comparing reconstructed ASL with altimetry

The reconstructed ASL (ASL$_r$) trend is compared to the altimetric ASL trend (ASL$_A$) in figure 5, while TG-based ASL (ASL$_\text{TG}$ trend is indicated with dots. Table 1 and figure 6 shows the sea level contributions estimated at each tide gauge. There is an overall agreement of the sea level trend pattern in both ASL$_r$ and ASL$_\text{A}$ The main obvious difference between the spatial sea level pattern of ASL$_r$ and ASL$_\text{A}$ is the larger sea level rise in the Beaufort Sea and sea level fall in the East-Siberian seas of ASL$_r$.

Before the era of SAR altimetry (from October 2010), the ability to separate the leads and the sea ice was more difficult due to the larger footprint of the conventional satellites. Therefore, in areas with a dense sea ice cover (like the Beaufort Sea), more altimetric observations exist during the sea level high of the autumn and fewer during winter/spring where sea level is lower (i.e. Armitage et al. (2016)). This creates a seasonal bias that is more pronounced before the CryoSat-2 era, because of the lower resolution in the pre-SAR era. This bias can explain the 'flattening' of the trend in the Beaufort Sea seen in figure 5), where ASL$_\text{A}$ shows a smaller doming of the Beaufort Gyre than ASL$_r$. From the time series (right panel of figure 5) is it evident that

ASL_A is higher than ASL_r from 2003-2009 and then shifts to a lower level after 2010. The same difference between ASL_r and ASL_A is not observed in a predominately non-SAR region of the Norwegian Sea. Another altimetry based SLA-estimate from 2003-2015 (Armitage et al., 2016), observes a larger trend in the Beaufort Gyre in alignment with the values of ASL_r.

In the altimetric estimate (middle panel of figure 5) a positive sea level trend extends in the Norwegian Sea until it reaches the average sea ice boundary, which (intentionally) coincides with the SAR-boundary of CryoSat-2. From altimetry it is unclear if this signal is a real physical signal or due to bias when different altimetric observations (different satellites and SAR/non-SAR), sea ice and open ocean regions are aligned in the DTU/TUM product or an error in the SAR-based DTU18MSS (Andersen et al., 2018) that is used as a reference in the altimetry data. From the ASL_r some of the positive sea level trends is restored in the Norwegian Sea by a combination of the thermosteric contribution (figure 3) and the negative gravitational contribution from Greenland (figure 4a). The boundary between sea ice and open ocean is however less significant in ASL_r and a spatial bias in altimetry cannot be excluded.

4.2 Comparing ASL-trends at tide gauge locations

TGs only measure sea level in coastal areas, and are therefore not useful when analyzing spatial sea level trend patterns of the Arctic Ocean. Furthermore, is the coastal location often disturbed by the local environment that might be unknown (e.g. small river outflow, local construction, packing of sea ice etc.), which can influence both sea level measurements from tide gauge and altimetry.

In figure 6 and table 1, the contributions to ASL_r is quantified at the location at each of the twelve TGs by taking the mean trend of a radius of 50 km (5 km for GIA and elastic VLM). This radius ensures, that Rorvik, Nome and Reykjavik overlaps the altimetric data, but the fewer number of data points might cause the data to be more variable and hence increase the uncertainty (estimated as standard error, σ).

The Norwegian tide gauges (Rorvik, Tromso, Vardo) are considered the most stable and also show the lowest error estimate (together with Ny-Ålesund). ASL_r is in good agreement with the tide gauge and is for Rorvik and Vardo in better alignment with ASL_{TG} than ASL_A. This is also the region with highest density of hydrographical data and thus the region with the most reliable steric estimate. We see that for Vardo and Rorvik, the sea level change is split between a steric and a mass contribution of roughly the same size, which is similar to the share of the global sea level trend (Church and White, 2011b; WCRP, 2018). At Tromso a negative halosteric trend (more saline water) is lowering ASL_r. However, ASL_r around Tromso (50-200 km) yields a better agreement with the observed ASL_{TG} and ASL_A.

The Siberian coast has multiple river outlets that contributes with freshwater of the Arctic Ocean (Proshutinsky et al., 2004; Morison et al., 2012; Armitage et al., 2016). A positive halosteric sea level trend is visible at the coast of the Bering and Kara Sea, where the river OB has a major outflow. At Amderma TG, which is located on the coast between the Barents and Kara Sea, but not near any major outflow, a significant halosteric trend is recognized by the TG-measured sea level, despite rather large uncertainties. Ice loss from Novaya Zemlya contributes with over 1 gigaton of freshwater to the Kara Sea every year and the ice loss has been accelerating (Melkonian et al., 2016), but the contribution is small compared to the +500 Gt coming from the rivers every year. The halosteric signal could (falsely) be extrapolated from the gulf of Ob which has major river outlets

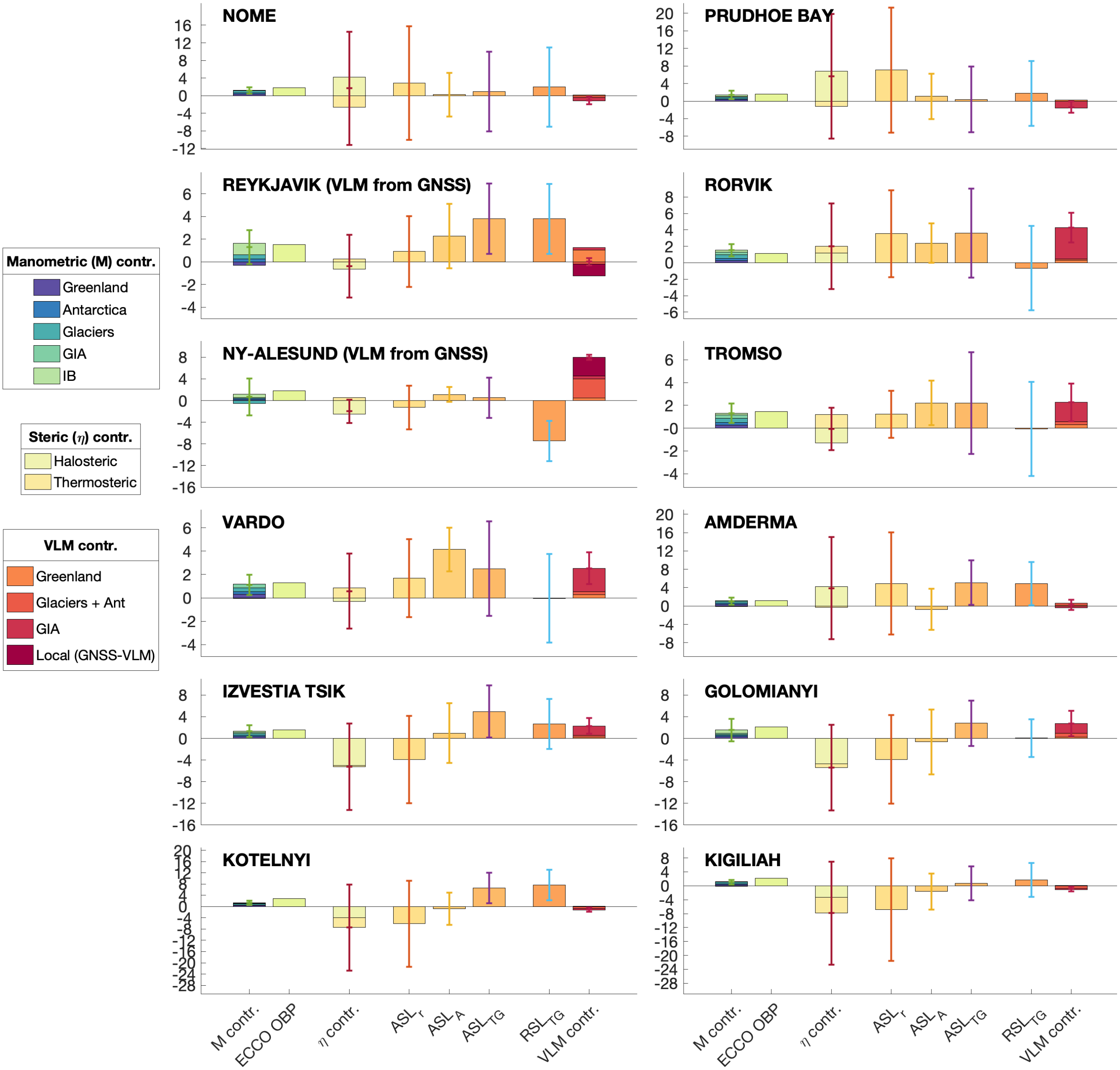

Figure 6. Components of sea level trend [mm y^{-1}] for each tide gauge from 1995-2015. The three bars in the middle (ASL_r, ASL_A and ASL_{TG}) are the three independent estimates of absolute sea level. The error bars indicate one standard error (combined error from each component when relevant). The VLM component 'Local (GNSS-VLM)' is only relevant at Reykjavik and Ny Ålesund, because significant local properties causes VLM that is not present in the VLM-model (Ludwigsen et al., 2020b). Glacier component of VLM includes the effect of rotational feedback, ocean loading, and Antarctica which are less than 0.5 mm y^{-1} combined.

	$\dot{\text{RSL}}_{\text{TG}}$	VLM (model/GNSS)	$\mathbf{\dot{ASL}_{TG}}$	IB	$\dot{N}$	$\dot{\text{M}}$	$\dot{\eta}$ $(\dot{\eta_S}+\dot{\eta_T})$	$\mathbf{\dot{ASL}_{\mathit{r}}}$	$\mathbf{\dot{ASL}_{\mathit{A}}}$
NOME	2.0 ± 9.0	-1.1 ± 0.9	**0.9 ± 9.1**	0.1	1.1 ± 0.7	1.2 ± 0.7	1.7 ± 12.9	**2.8 ± 12.9**	**0.2 ± 4.9**
PRUDHOE BAY	1.7 ± 7.4	-1.4 ± 1.3	**0.4 ± 7.5**	0.4	1.0 ± 0.9	1.4 ± 0.9	5.7 ± 14.2	**7.1 ± 14.2**	**1.1 ± 5.2**
REYKJAVIK	3.8 ± 3.1	0.0 ± 0.3	**3.8 ± 3.1**	1.0	0.3 ± 1.5	1.3 ± 1.5	-0.4 ± 2.8	**0.9 ± 3.1**	**2.3 ± 2.8**
RORVIK	-0.7 ± 5.1	4.3 ± 1.8	**3.6 ± 5.4**	0.3	1.3 ± 0.7	1.5 ± 0.7	2.0 ± 5.2	**3.5 ± 5.3**	**2.4 ± 2.4**
NY-ALESUND	-7.4 ± 3.7	8.0 ± 0.5	**0.5 ± 3.7**	0.6	0.1 ± 3.4	0.7 ± 3.4	-2.0 ± 2.2	**-1.3 ± 4.0**	**1.1 ± 1.4**
TROMSO	-0.1 ± 4.1	2.3 ± 1.7	**2.2 ± 4.4**	0.1	1.1 ± 0.9	1.3 ± 0.9	-0.1 ± 1.9	**1.2 ± 2.1**	**2.2 ± 1.9**
VARDO	-0.0 ± 3.8	2.5 ± 1.4	**2.5 ± 4.0**	-0.1	1.2 ± 0.9	1.1 ± 0.9	0.6 ± 3.2	**1.7 ± 3.3**	**4.1 ± 1.9**
AMDERMA	4.9 ± 4.7	0.2 ± 1.1	**5.1 ± 4.9**	-0.1	1.1 ± 0.8	1.0 ± 0.8	3.9 ± 11.1	**4.9 ± 11.2**	**-0.8 ± 4.5**
IZVESTIA TSIK	2.7 ± 4.6	2.3 ± 1.5	**5.0 ± 4.8**	0.2	1.1 ± 1.1	1.3 ± 1.1	-5.2 ± 8.0	**-3.9 ± 8.0**	**1.0 ± 5.5**
GOLOMIANYI	0.0 ± 3.5	2.8 ± 2.3	**2.8 ± 4.2**	0.6	0.9 ± 2.1	1.5 ± 2.1	-5.4 ± 7.9	**-3.9 ± 8.2**	**-0.7 ± 6.0**
KOTELNYI	7.7 ± 5.4	-1.1 ± 0.8	**6.5 ± 5.4**	0.2	1.1 ± 0.7	1.4 ± 0.7	-7.5 ± 15.3	**-6.1 ± 15.3**	**-0.8 ± 5.7**
KIGILIAH	1.7 ± 4.8	-0.9 ± 0.7	**0.8 ± 4.9**	-0.1	1.2 ± 0.7	1.0 ± 0.7	-7.9 ± 14.8	**-6.8 ± 14.8**	**-1.6 ± 5.1**

Table 1. 1995-2015 sea level trends [mm y^{-1}] at the 12 tide gauge locations. The trends (least-squares) are generally based on a annual mean-value of a 50 km radius around the tide gauge. For VLM a 5 km radius is used, except for Ny-Alesund and Reykjavik where VLM is based on GNSS-measurements. The columns in bold indicate the three estimates of Absolute Sea Level ($\dot{\text{ASL}}_{\text{TG}}$, $\dot{\text{ASL}}_r$ and $\dot{\text{ASL}}_A$).

and the agreement with ASL_{TG} is accidental. So the reason for this halosteric sea level rise at Anderma is remains unclear. In any case, both ASL_{TG} and ASL_r is in opposition to altimetry observations that shows a negative ASL-trend.

Further east along the Siberian coast the four TGs (Izvestia Tsik, Golomianyi, Kotelnyi, Kigiliah) all show a rising ASL, while both ASL_{A} and in particular ASL_r shows a negative trend in the region. Even though the ECCO OBP is 1-2 mm y^{-1} higher than the manometric estimate (figure 4) it is not enough to explain the discrepancy between ASL_{TG} and ASL_r but explains some of the ASL_A/ASL_r difference. Figure 3 shows that a negative halosteric sea level trend is dominating the reconstructed sea level trend in the region, but the poor hydrographic coverage along the Siberian coast (Ludwigsen and Andersen, 2020) makes the uncertainty of the halosteric trend large. This negative steric sea level trend is however supported by the results of Armitage and Davidson (2014) from combining GRACE with altimetry. They estimate a steric sea level in the Siberian Arctic (excluding the Barents Sea) in the order of -5 mm y^{-1} from 2003 to 2014, which is same order of the estimated steric trend of this study in the region.

The positive ASL trend among tide gauges in the eastern Russian Arctic is however consistent and has been recognized in other studies using an extended set of Russian tide gauges (Proshutinsky et al., 2004; Henry et al., 2012). Remarkably is that the TG-trend at Kotelnyi and Kigiliah differ with almost 6 mm y^{-1} (in total 12 cm difference over the time span of this study) despite being less than 250 km apart. This gradient is only reasonable, if local circumstances that affects the RSL is considered. Local coastal subsidence not associated with land ice loss/gain, i.e. caused by thawing of permafrost or oil depletion, is a possible explanation.

Nome and Prudhoe Bay in Alaska both show a positive steric trend which is not reflected in sea level trends from altimetry or the tide gauge, thus resulting in a rather large discrepancy between ASL_r and $\text{ASL}_{\text{A/TG}}$. The strong halosteric trend of the

Beaufort Gyre, might be extrapolated towards the Alaskan coastline and into the Bering Strait in the DTU steric model. There is no evidence in the literature for a extent of the Beaufort Gyre doming as shown from the halosteric trend, which indicates, that the weighted spatial interpolation in combination with higher hydrographic data density in the Beaufort Sea creates this widening of the Beaufort Gyre.

Ny-Ålesund on Svalbard is dominated by a large VLM caused by recent deglaciation. This uplift completely mitigates the large sea level fall measured by the tide gauge and results in small rise of $\mathrm{ASL_{TG}}$. In (Ludwigsen et al., 2020a) it is argued that the discrepancy between GNSS and the VLM-model in large originates from VLM because of post-LIA deglaciation on Svalbard (Rajner, 2018). This viscoelastic GIA-like LIA-effect will certainly also have a gravitational sea level fingerprint ($\dot{N}$) that should be added to the manometric sea level change $\dot{\mathrm{M}}$. This can explain some of the difference between ASL_r and $\mathrm{ASL_{A/TG}}$. A possibly positive dynamic $\dot{\mathrm{M}}$-change (from the (ECCO OBP)$-\dot{\mathrm{M}}$ difference in figure 4h) could further close the $\mathrm{ASL}_r - \mathrm{ASL_{A/TG}}$ gap.

From the calculations of the gravitational fingerprint, none of the TG-sites in this study experience a net sea level fall from contemporary deglaciation and GIA ($\dot{N}$ in table 1) and only Ny-Ålesund (-0.4 mm y^{-1}) and Reykjavik (-0.2 mm y^{-1}) will experience a small sea level fall from contemporary deglaciation alone. So even though the Arctic is heavily prone to ice mass loss and thus a smaller gravitational pull, the Arctic as a region is not experiencing a absolute sea level fall from comtemporary deglaciation. On the contrary, it causes the sea level to rise with around 1 mm y^{-1} in most of the Arctic. However, by accounting for the deglaciation effect on VLM, the RSL-change from contemporary deglaciation will be negative in large areas of the Arctic.

5 Uncertainty and assessment of ASL-trends

The uncertainties of the trend estimates for $\mathrm{RSL_{TG}}$, VLM, gravitational fingerprint (N), steric (η) in table 1 and figure 6 are derived as the standard error (σ) of the detrended timeseries of the annual mean values. GIA (Caron et al., 2018) and altimetry (Rose et al., 2019) has a associated uncertainty that is used. In the case of VLM a 10% error is added to account for uncertainties of the earth model (Wang et al., 2012).

The spatial distribution of the uncertainties are shown in figure 7. Generally, the largest uncertainties are found along the Siberian coast and in the interior of the Arctic where the largest sea level trend is present. The steric uncertainty is in most cases the largest source of uncertainty (figure 6). The standard error naturally reflects if the steric heights are unstable and poorly constrained (if for example there are few hydro-graphic data). In principle, this method requires temporal independence, which is not entirely true, since outliers are replaced with data from adjacent years. Furthermore, large influence by the non-periodic and non-linear Arctic Oscillation, would enhance the uncertainty, even though this is a real physical signal. Thereby is the estimated error a composite of uncertainties originating from the way the sea level component is constructed and from, the sometimes large, interannual variability.

The mass contribution and VLM has naturally the largest uncertainties close to glaciated areas. Glacial ice loss on Baffin Island is poorly constrained in the ice model, which is reflected with large uncertainties in this area. The uncertainty of altimetry

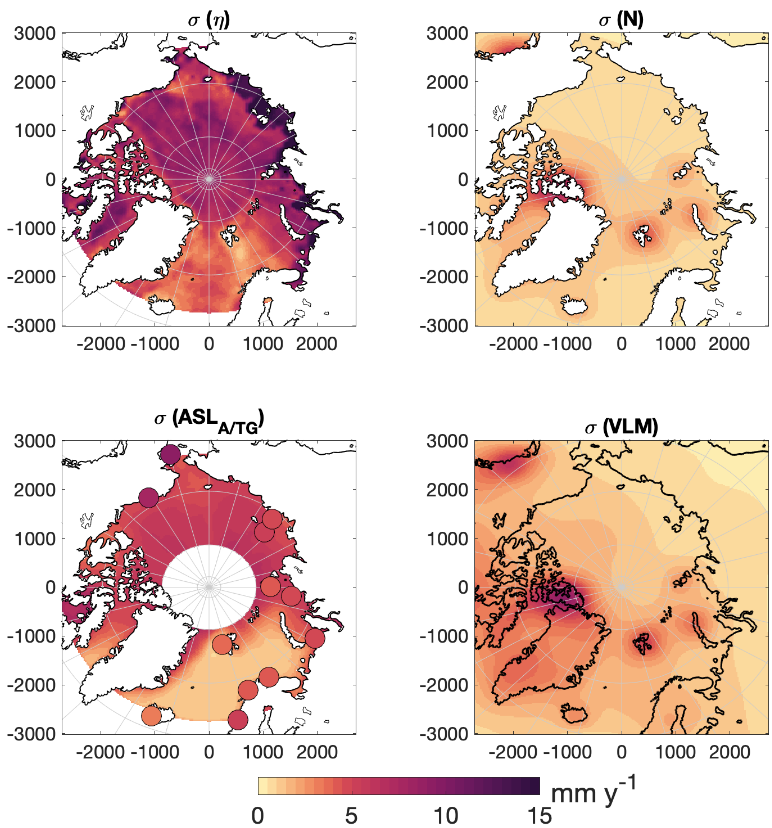

Figure 7. Standard error (1 σ) of the 1995-2015 trend [mm y^{-1}] for combined steric, combined $\dot{N}$, $ASL_{A/TG}$ and combined VLM contributions.

is reflecting the data availability of areas with sea ice contrary the ice-free ocean, while the largest uncertainties of the TGs are those with largest interannual variability.

Left map of figure 8 shows the difference between ASL_r and $ASL_{A/TG}$. The pattern somehow resembles the trend of the halosteric contribution, which reflects the halosteric dominance of the spatial variability. The correlation coefficient (R) between ASL_r and ASL_A is R=0.50 (R=0.23 without the halosteric contribution) and R=0.53 when using the ECCO OBP estimate instead of the reconstructed manometric sea level. The correlation is better than the correlation coefficients reached by (Ludwigsen and Andersen, 2020), where they used different datasets of GRACE (R=0.19-0.40) combined with the same steric and altimetric datasets. From the middle panel in figure 8 we see that for most of the Arctic (78%) and for 8 of 12 TGs, the absolute difference is less than half of the combined standard error and in 98% of the area, is ASL_r in agreement with ASL_A within the associated uncertainty, which indicates that the error is a conservative estimate. Only the TG Izvestia Tsik shows a larger difference between observed (ASL_{TG}) and reconstructed sea level (ASL_r) than the associated standard error.

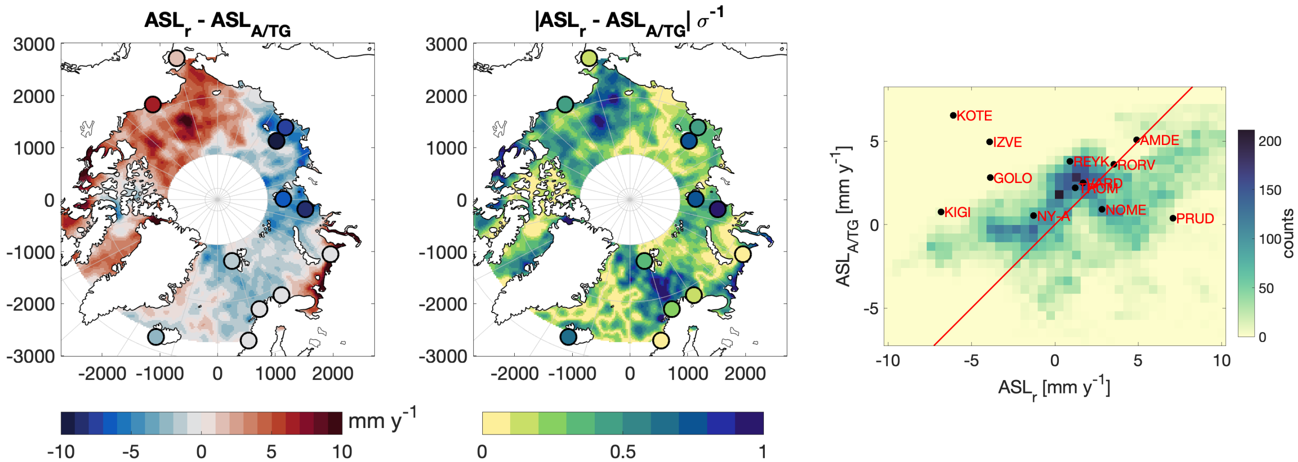

Figure 8. Left map shows the difference between ASL_r and $\mathrm{ASL}_{\mathrm{A/TG}}$. Middle map is the absolute difference divided by the standard error from 7 (combined uncertainty). Right panel shows a correlation matrix between ASL_r and $\mathrm{ASL}_{\mathrm{A/TG}}$. The color indicates the number of data grid cells falling into bin size of 0.5 mm y^{-1}. 96% of the grid cells with data is covered within the bounds of the matrix ($\mathrm{N}_{\mathrm{total}}$=18150). The red line is where ASL_r is equal to $\mathrm{ASL}_{\mathrm{A/TG}}$.

The right panel of figure 8 shows the correlation matrix between observed ASL ($\mathrm{ASL}_{\mathrm{A/TG}}$) and reconstructed ASL (ASL_r). The matrix shows that ASL_r and $\mathrm{ASL}_{\mathrm{A}}$ are largely correlated. There is large accumulation around 2 mm y^{-1}, with slightly higher $\mathrm{ASL}_{\mathrm{A}}$ than ASL_r. This originates from the underestimate of the ASL-reconstruction (see figure 8) in the Norwegian Sea and the difference agrees with the ECCO OBP-$\dot{\mathrm{M}}$ difference (figure 4h) and thus likely explained by the missing dynamic sea level contribution of $\dot{\mathrm{M}}$. Evident are also the large positive ASL_r-trends from the Beaufort Sea and negative ASL_r-trends along the Siberian Coast that is not reflected in ASL_A.

6 Conclusion

All significant contributions to the sea level change from 1995-2015 in the Arctic Ocean were mapped and assessed at 12 tide gauges located throughout the Arctic Ocean. This was done for the first time without the use of GRACE data or modeled steric data. Thereby are we able to reconstruct the Arctic absolute sea level change and attribute the changes to their origin and thus understand the causes behind the altimetry and TG-observed sea level trend. By using a VLM-model, that includes both GIA and elastic uplift, the TG-observed sea level can be utilized in locations where no reliable GNSS-data is present.

From figure 5 we clearly see that the general spatial pattern of altimetry observed sea level ($\mathrm{ASL}_{\mathrm{A}}$) is restored in the reconstructed ASL-estimate (ASL_r). The correlation (R=0.50) outperforms GRACE-based sea level budget assessments from (Ludwigsen and Andersen, 2020) (R=0.19-0.40). Figure 6 and 7 show that steric sea level dominates the spatial variability.

This is also the main source of uncertainty, while manometric sea level change has a more uniform and smaller contribution to ASL. Some areas, in particular, the Norwegian Sea, has more observations (from both altimetry and hydrographic data) and thus can the individual contributions be estimated with lower uncertainty. The Siberian Seas are however poorly constrained with observations and both the steric product, altimetry and tide gauges show large uncertainties. Figure 8 shows the spatial agreement between observed sea level ($ASL_{A/TG}$) and the reconstructed ASL estimate within the combined uncertainty. The reconstructed ASL-estimate agrees with altimetry in 98% of the area and 11 of the 12 TGs within the uncertainty.

The correlation between the reconstructed sea level and altimetry is significant (R=0.50), but also shows that the sea level budget is not closed or completely understood everywhere in the Arctic - likely because of poorly constrained steric data and a uncertain dynamic contribution that is difficult to reconstruct. However, the reconstructed sea level confirms the negative halosteric-driven sea level trend along the east Siberian coast identified by (Armitage and Davidson, 2014), which is in contrast to the TG-observed sea level in the region. Large variations among TGs in East Siberia indicate very local VLM affecting the TG-observed RSL.

From figure 8 we see that the uncertainties in most of the Arctic are significantly larger than the difference between the reconstructed sea level and altimetry. This is including most of the Siberian Seas, indicating that the uncertainty of the components of this study of the sea level trend might be a conservative estimate. Better constrained estimates of both the manometric and steric sea level are necessary to get a complete understanding of what changes Arctic sea level and to validate sea level trends observed by altimetry, which are not necessarily more accurate than the derived ASL-estimates.

Code and data availability. Tide gauge sea level timeseries is available at psmsl.org, the VLM-model available at data.dtu.dk/articles/dataset/Arctic_Vertical_Land_Motion_5x5_km, DTU Steric is available at ftp.space.dtu.dk/pub/DTU19/STERIC/, the REAR-software is available at github at github.com/danielemelini/rear.git.

Author contributions. CAL: Method, concept, data analysis and writing. OBA: Concept and editing. SKR: Providing altimetry data, validation and editing.

Competing interests. The authors declare no competing interests.

Acknowledgements. The authors want to thank two anonymous reviewers for their comments that greatly improved the manuscript. Furthermore, we thank Lambert Caron for providing the Caron2018 GIA-model, available at https://vesl.jpl.nasa.gov/solid-earth/gia/ and Danielle Melini for creating the REAR-code (Melini et al., 2015). This research was funded by the EU-INTAROS project (Grant agreement no. 727890) (CAL and OBA) and by the ESA-Climate Change Initiative Sea level budget closure (Expro RFP/3-14679/16/INB) (OBA and SKR).

References

Andersen, O., Knudsen, P., and Stenseng, L.: A New DTU18 MSS Mean Sea Surface – Improvement from SAR Altimetry, p. 172, 25 years of progress in radar altimetry symposium ; Conference date: 24-09-2018 Through 29-09-2018, 2018.

Armitage, T. W. K. and Davidson, M. W. J.: Using the Interferometric Capabilities of the ESA CryoSat-2 Mission to Improve the Accuracy of Sea Ice Freeboard Retrievals, IEEE Transactions on Geoscience and Remote Sensing, 52, 529–536, 2014.

Armitage, T. W. K., Bacon, S., Ridout, A. L., Thomas, S. F., Aksenov, Y., and Wingham, D. J.: Arctic sea surface height variability and change from satellite radar altimetry and GRACE, 2003–2014, Journal of Geophysical Research: Oceans, 121, 4303–4322, https://doi.org/10.1002/2015JC011579, https://agupubs.onlinelibrary.wiley.com/doi/abs/10.1002/2015JC011579, 2016.

Armitage, T. W. K., Bacon, S., and Kwok, R.: Arctic Sea Level and Surface Circulation Response to the Arctic Oscillation, Geophysical Research Letters, 45, 6576–6584, https://doi.org/10.1029/2018GL078386, https://agupubs.onlinelibrary.wiley.com/doi/abs/10.1029/2018GL078386, 2018.

Bamber, J. and Riva, R.: The sea level fingerprint of recent ice mass fluxes, The Cryosphere, 4, 621–627, https://doi.org/10.5194/tc-4-621-2010, https://www.the-cryosphere.net/4/621/2010/, 2010.

Behrendt, A., Sumata, H., Rabe, B., and Schauer, U.: A comprehensive, quality-controlled and up-to-date data set of temperature and salinity data for the Arctic Mediterranean Sea (Version 1.0), links to data files, https://doi.org/10.1594/PANGAEA.872931, https://doi.org/10.1594/PANGAEA.872931, supplement to: Behrendt, A et al. (2017): UDASH - Unified Database for Arctic and Subarctic Hydrography. Earth System Science Data Discussions, 37 pp, https://doi.org/10.5194/essd-2017-92, 2017.

Box, J. E., Colgan, W. T., Christensen, T. R., Schmidt, N. M., Lund, M., Parmentier, F. J. W., Brown, R., Bhatt, U. S., Euskirchen, E. S., Romanovsky, V. E., Walsh, J. E., Overland, J. E., Wang, M., Corell, R. W., Meier, W. N., Wouters, B., Mernild, S., Mård, J., Pawlak, J., and Olsen, M. S.: Key indicators of Arctic climate change: 1971-2017, Environmental Research Letters, 14, 045 010, https://doi.org/10.1088/1748-9326/aafc1b, 2019.

Calafat, F. M., Chambers, D. P., and Tsimplis, M. N.: Mechanisms of decadal sea level variability in the eastern North Atlantic and the Mediterranean Sea, Journal of Geophysical Research: Oceans, 117, https://doi.org/10.1029/2012JC008285, https://agupubs.onlinelibrary.wiley.com/doi/abs/10.1029/2012JC008285, 2012.

Caron, L., Ivins, E. R., Larour, E., Adhikari, S., Nilsson, J., and Blewitt, G.: GIA Model Statistics for GRACE Hydrology, Cryosphere, and Ocean Science, Geophysical Research Letters, 45, 2203–2212, https://doi.org/10.1002/2017GL076644, https://agupubs.onlinelibrary.wiley.com/doi/abs/10.1002/2017GL076644, 2018.

Carret, A., Johannessen, J. A., Andersen, O. B., Ablain, M., Prandi, P., Blazquez, A., and Cazenave, A.: Arctic Sea Level During the Satellite Altimetry Era, Surveys in Geophysics, 38, 251–275, https://doi.org/10.1007/s10712-016-9390-2, https://doi.org/10.1007/s10712-016-9390-2, 2017.

Cheng, Y., Andersen, O., and Knudsen, P.: An Improved 20-Year Arctic Ocean Altimetric Sea Level Data Record, Marine Geodesy, 38, 146–162, https://doi.org/10.1080/01490419.2014.954087, 2015.

Church, J. and White, N.: Sea-Level Rise from the Late 19th to the Early 21st Century, Surveys in Geophysics, 32, 585–602, https://doi.org/10.1007/s10712-011-9119-1, https://www.scopus.com/inward/record.uri?eid=2-s2.0-80053195533&doi=10.1007%2fs10712-011-9119-1&partnerID=40&md5=a6a2b9bb53f622e9bf4b3266a27d54f0, cited By 737, 2011a.

Church, J. A. and White, N. J.: Sea-Level Rise from the Late 19th to the Early 21st Century, Surveys in Geophysics, 32, 585–602, https://doi.org/10.1007/s10712-011-9119-1, https://doi.org/10.1007/s10712-011-9119-1, 2011b.

Dangendorf, S., Hay, C., Calafat, F. M., Marcos, M., Piecuch, C. G., Berk, K., and Jensen, J.: Persistent acceleration in global sea-level rise since the 1960s, Nature Climate Change, 9, 705–710, https://doi.org/10.1038/s41558-019-0531-8, 2019.

Forget, G., Campin, J.-M., Heimbach, P., Hill, C. N., Ponte, R. M., and Wunsch, C.: ECCO version 4: an integrated framework for non-linear inverse modeling and global ocean state estimation, Geoscientific Model Development, 8, 3071–3104, https://doi.org/10.5194/gmd-8-3071-2015, https://gmd.copernicus.org/articles/8/3071/2015/, 2015.

Frederikse, T., Jevrejeva, S., Riva, R., and Dangendorf, S.: A consistent sea-level reconstruction and its budget on basin and global scales over 1958-2014, Journal of Climate, 31, 1267–1280, https://doi.org/10.1175/JCLI-D-17-0502.1, https://www.scopus.com/inward/record.uri?eid=2-s2.0-85040922795&doi=10.1175%2fJCLI-D-17-0502.1&partnerID=40&md5=3a2c9a8327f26f947827ce721d43c5d4, cited By 12, 2018.

Frederikse, T., Landerer, F., Caron, L., Adhikari, S., Parkes, D., Humphrey, V. W., Dangendorf, S., Hogarth, P., Zanna, L., Cheng, L., and Wu, Y. H.: The causes of sea-level rise since 1900, Nature, 584, 393–397, https://doi.org/10.1038/s41586-020-2591-3, 2020.

Fukumori, I., Wang, O., Fenty, I., Forget, G., Heimbach, P., and Ponte, R. M.: ECCO Version 4 Release 4 Dataset, accessed: 2020-06-25, 2019.

Gill, A. and Niller, P.: The theory of the seasonal variability in the ocean, Deep Sea Research and Oceanographic Abstracts, 20, 141 – 177, https://doi.org/https://doi.org/10.1016/0011-7471(73)90049-1, http://www.sciencedirect.com/science/article/pii/0011747173900491, 1973.

Gregory, J. M., Griffies, S. M., Hughes, C. W., Lowe, J. A., Church, J. A., Fukimori, I., Gomez, N., Kopp, R. E., Landerer, F., Cozannet, G. L., Ponte, R. M., Stammer, D., Tamisiea, M. E., and van de Wal, R. S. W.: Concepts and Terminology for Sea Level: Mean, Variability and Change, Both Local and Global, Surveys in Geophysics, 40, 1251–1289, https://doi.org/10.1007/s10712-019-09525-z, https://doi.org/10.1007/s10712-019-09525-z, 2019.

Henry, O., Prandi, P., Llovel, W., Cazenave, A., Jevrejeva, S., Stammer, D., Meyssignac, B., and Koldunov, N.: Tide gauge-based sea level variations since 1950 along the Norwegian and Russian coasts of the Arctic Ocean: Contribution of the steric and mass components, Journal of Geophysical Research: Oceans, 117, https://doi.org/10.1029/2011JC007706, https://agupubs.onlinelibrary.wiley.com/doi/abs/10.1029/2011JC007706, 2012.

Holgate, S. J., Matthews, A., Woodworth, P. L., Rickards, L. J., Tamisiea, M. E., Bradshaw, E., Foden, P. R., Gordon, K. M., Jevrejeva, S., and Pugh, J.: New Data Systems and Products at the Permanent Service for Mean Sea Level, Journal of Coastal Research, 29, 493–504, https://doi.org/10.2112/JCOASTRES-D-12-00175.1, https://doi.org/10.2112/JCOASTRES-D-12-00175.1, 2012.

Khan, S. A., Sasgen, I., Bevis, M., van Dam, T., Bamber, J. L., Wahr, J., Willis, M., Kjær, K. H., Wouters, B., Helm, V., Csatho, B., Fleming, K., Bjørk, A. A., Aschwanden, A., Knudsen, P., and Munneke, P. K.: Geodetic measurements reveal similarities between post–Last Glacial Maximum and present-day mass loss from the Greenland ice sheet, Science Advances, 2, https://doi.org/10.1126/sciadv.1600931, https://advances.sciencemag.org/content/2/9/e1600931, 2016.

King, M. A., Keshin, M., Whitehouse, P. L., Thomas, I. D., Milne, G., and Riva, R. E. M.: Regional biases in absolute sea-level estimates from tide gauge data due to residual unmodeled vertical land movement, Geophysical Research Letters, 39, https://doi.org/10.1029/2012GL052348, https://agupubs.onlinelibrary.wiley.com/doi/abs/10.1029/2012GL052348, 2012.

Kustowski, B., Dziewon´ski, A. M., and Ekstro¨m, G.: Nonlinear Crustal Corrections for Normal-Mode Seismograms, Bulletin of the Seismological Society of America, 97, 1756–1762, https://doi.org/10.1785/0120070041, https://doi.org/10.1785/0120070041, 2007.

Laxon, S., Peacock, H., and Smith, D.: High interannual variability of sea ice thickness in the Arctic region, Nature, 425, 947–950, https://doi.org/10.1038/nature02050, 2003.

Limkilde Svendsen, P., Andersen, O. B., and Aasbjerg Nielsen, A.: Stable reconstruction of Arctic sea level for the 1950–2010 period, Journal of Geophysical Research: Oceans, 121, 5697–5710, https://doi.org/10.1002/2016JC011685, https://agupubs.onlinelibrary.wiley.com/doi/abs/10.1002/2016JC011685, 2016.

Ludwigsen, C., Khan, S. A., Andersen, O. B., and Marzeion, B.: Vertical Land Motion from present-day deglaciation in the wider Arctic, Earth and Space Science Open Archive, p. 18, https://doi.org/10.1002/essoar.10502890.1, https://doi.org/10.1002/essoar.10502890.1, 2020a.

Ludwigsen, C. A. and Andersen, O. B.: Contributions to Arctic sea level from 2003 to 2015, Advances in Space Research, https://doi.org/https://doi.org/10.1016/j.asr.2019.12.027, http://www.sciencedirect.com/science/article/pii/S0273117719309275, 2020.

Ludwigsen, C. A., Andersen, O. B., Khan, S. A., and Marzeion, B.: Arctic Vertical Land Motion (5x5 km), https://doi.org/10.11583/DTU.12554489.v1, https://data.dtu.dk/articles/dataset/Arctic_Vertical_Land_Motion_5x5_km_/12554489, 2020b.

Luthcke, S. B., Sabaka, T., Loomis, B., Arendt, A., McCarthy, J., and Camp, J.: Antarctica, Greenland and Gulf of Alaska land-ice evolution from an iterated GRACE global mascon solution, Journal of Glaciology, 59, 613–631, https://doi.org/10.3189/2013JoG12J147, 2013.

Marzeion, B., Jarosch, A. H., and Hofer, M.: Past and future sea-level change from the surface mass balance of glaciers, The Cryosphere, 6, 1295–1322, https://doi.org/10.5194/tc-6-1295-2012, https://www.the-cryosphere.net/6/1295/2012/, 2012.

Melini, D., Spada, G., Gegout, P., and King, M.: REAR: a Regional ElAstic Rebound calculator. User manual for version 1.0, available on–line at: http://hpc.rm.ingv.it/rear., 2015.

Melkonian, A. K., Willis, M. J., Pritchard, M. E., and Stewart, A. J.: Recent changes in glacier velocities and thinning at Novaya Zemlya, Remote Sensing of Environment, 174, 244 – 257, https://doi.org/https://doi.org/10.1016/j.rse.2015.11.001, http://www.sciencedirect.com/science/article/pii/S0034425715301899, 2016.

Morison, J., Kwok, R., Peralta-Ferriz, C., Alkire, M., Rigor, I., Andersen, R., and Steele, M.: Changing Arctic Ocean freshwater pathways, Nature, 481, 66–70, https://doi.org/10.1038/nature10705, https://doi.org/10.1038/nature10705, 2012.

Naeije, M., Schrama, E., and Scharroo, R.: The radar Altimeter Database System project RADS, 2, 487 – 490 vol.2, https://doi.org/10.1109/IGARSS.2000.861605, 2000.

Peacock, N. R. and Laxon, S. W.: Sea surface height determination in the Arctic Ocean from ERS altimetry, Journal of Geophysical Research C: Oceans, 109, C07 001 1–14, https://doi.org/10.1029/2001JC001026, 2004.

Peltier, W.: Closure of the budget of global sea level rise over the GRACE era: the importance and magnitudes of the required corrections for global glacial isostatic adjustment, Quaternary Science Reviews, 28, 1658 – 1674, https://doi.org/https://doi.org/10.1016/j.quascirev.2009.04.004, http://www.sciencedirect.com/science/article/pii/S0277379109001218, quaternary Ice Sheet-Ocean Interactions and Landscape Responses, 2009.

Prandi, P., Ablain, M., Cazenave, A., and Picot, N.: A New Estimation of Mean Sea Level in the Arctic Ocean from Satellite Altimetry, Marine Geodesy, 35, 61–81, https://doi.org/10.1080/01490419.2012.718222, https://doi.org/10.1080/01490419.2012.718222, 2012.

Proshutinsky, A., Ashik, I. M., Dvorkin, E. N., Häkkinen, S., Krishfield, R. A., and Peltier, W. R.: Secular sea level change in the Russian sector of the Arctic Ocean, Journal of Geophysical Research: Oceans, 109, https://doi.org/10.1029/2003JC002007, https://agupubs.onlinelibrary.wiley.com/doi/abs/10.1029/2003JC002007, 2004.

Pugh, D. and Woodworth, P.: Sea-Level Science: Understanding Tides, Surges, Tsunamis and Mean Sea-Level Changes, Cambridge University Press, https://doi.org/10.1017/CBO9781139235778, 2014.

Raj, R. P., Andersen, O. B., Johannessen, J. A., Gutknecht, B. D., Chatterjee, S., Rose, S. K., Bonaduce, A., Horwath, M., Ranndal, H., Richter, K., Palanisamy, H., Ludwigsen, C. A., Bertino, L., Nilsen, J. E. O., Knudsen, P., Hogg, A., Cazenave, A., and Benveniste, J.: Arctic Sea level Budget Assessment During the GRACE/Argo Time Period, Remote Sensing, 12, https://doi.org/10.3390/rs12172837, https://www.mdpi.com/2072-4292/12/17/2837, 2020.

Rajner, M.: Detection of ice mass variation using gnss measurements at Svalbard, Journal of Geodynamics, 121, 20 – 25, https://doi.org/https://doi.org/10.1016/j.jog.2018.06.001, http://www.sciencedirect.com/science/article/pii/S0264370718300450, 2018.

Ricker, R., Hendricks, S., and Beckers, J. F.: The impact of geophysical corrections on sea-ice freeboard retrieved from satellite altimetry, Remote Sensing, 8, 317, https://doi.org/10.3390/rs8040317, 2016.

Roquet, F., Madec, G., McDougall, T. J., and Barker, P. M.: Accurate polynomial expressions for the density and specific volume of seawater using the TEOS-10 standard, Ocean Modelling, 90, 29 – 43, https://doi.org/https://doi.org/10.1016/j.ocemod.2015.04.002, http://www.sciencedirect.com/science/article/pii/S1463500315000566, 2015.

Rose, S. K., Andersen, O., Passaro, M., Ludwigsen, C., and Schwatke, C.: Arctic Ocean Sea Level Record from the Complete Radar Altimetry Era: 1991-2018, Remote Sensing, 11, https://doi.org/10.3390/rs11141672, 2019.

Royston, S., Dutt Vishwakarma, B., Westaway, R., Rougier, J., Sha, Z., and Bamber, J.: Can We Resolve the Basin-Scale Sea Level Trend Budget From GRACE Ocean Mass?, Journal of Geophysical Research: Oceans, 125, e2019JC015 535, https://doi.org/https://doi.org/10.1029/2019JC015535, https://agupubs.onlinelibrary.wiley.com/doi/abs/10.1029/2019JC015535, e2019JC015535 10.1029/2019JC015535, 2020.

Save, H., Bettadpur, S., and Tapley, B. D.: High-resolution CSR GRACE RL05 mascons, Journal of Geophysical Research: Solid Earth, 121, 7547–7569, https://doi.org/10.1002/2016JB013007, https://agupubs.onlinelibrary.wiley.com/doi/abs/10.1002/2016JB013007, 2016.

Schröder, L., Horwath, M., Dietrich, R., Helm, V., van den Broeke, M. R., and Ligtenberg, S. R. M.: Four decades of Antarctic surface elevation changes from multi-mission satellite altimetry, The Cryosphere, 13, 427–449, https://doi.org/10.5194/tc-13-427-2019, https://www.the-cryosphere.net/13/427/2019/, 2019.

Shepherd, A., Ivins, E., Rignot, E., Smith, B., van den Broeke, M., Velicogna, I., Whitehouse, P. L., Briggs, K., Joughin, I., Krinner, G., Nowicki, S., Payne, T., Scambos, T., Schlegel, N., A, G., Agosta, C., Ahlstrøm, A., Babonis, G., Barletta, V., Blazquez, A., Bonin, J., Csatho, B., Cullather, R., Felikson, D., Fettweis, X., Forsberg, R., Gallee, H., Gardner, A., Gilbert, L., Groh, A., Gunter, B., Hanna, E., Harig, C., Helm, V., Horvath, A., Horwath, M., Khan, S., K. Kjeldsen, K., Konrad, H., Langen, P., Lecavalier, B., Loomis, B., Luthcke, S., McMillan, M., Melini, D., Mernild, S., Mohajerani, Y., Moore, P., Mouginot, J., Moyano, G., Muir, A., Nagler, T., Nield, G., Nilsson, J., Noel, B., Otosaka, I., E. Pattle, M., Peltier, W. R., Pie, N., Rietbroek, R., Rott, H., Sandberg-Sørensen, L., Sasgen, I., Save, H., Scheuchl, B., Schrama, E., Schröder, L., Seo, K.-W., Simonsen, S., Slater, T., Spada, G., Sutterley, T., Talpe, M., Tarasov, L., van de Berg, W. J., van der Wal, W., van Wessem, M., Dutt Vishwakarma, B., Wiese, D., and Wouters, B.: Mass balance of the Antarctic Ice Sheet from 1992 to 2017, Nature, 558, 219–222, https://doi.org/10.1038/s41586-018-0179-y, 2018.

Shepherd, A., Ivins, E., Rignot, E., Smith, B., van den Broeke, M., Velicogna, I., Whitehouse, P., Briggs, K., Joughin, I., Krinner, G., Nowicki, S., Payne, T., Scambos, T., Schlegel, N., Geruo, A., Agosta, C., Ahlstrøm, A., Babonis, G., Barletta, V. R., Bjørk, A. A., Blazquez, A., Bonin, J., Colgan, W., Csatho, B., Cullather, R., Engdahl, M. E., Felikson, D., Fettweis, X., Forsberg, R., Hogg, A. E., Gallee, H., Gardner, A., Gilbert, L., Gourmelen, N., Groh, A., Gunter, B., Hanna, E., Harig, C., Helm, V., Horvath, A., Horwath, M., Khan, S., Kjeldsen, K. K., Konrad, H., Langen, P. L., Lecavalier, B., Loomis, B., Luthcke, S., McMillan, M., Melini, D., Mernild, S., Mohajerani, Y., Moore, P., Mottram, R., Mouginot, J., Moyano, G., Muir, A., Nagler, T., Nield, G., Nilsson, J., Noël, B., Otosaka, I., Pattle, M. E., Peltier, W. R., Pie, N., Rietbroek, R., Rott, H., Sørensen, L. S., Sasgen, I., Save, H., Scheuchl, B., Schrama, E., Schröder, L., Seo, K.-W., Simonsen, S. B., Slater, T., Spada, G., Sutterley, T., Talpe, M., Tarasov, L., Jan van de Berg, W., van der Wal, W., van Wessem, M., Vishwakarma, B. D., Wiese, D., Wilton, D., Wagner, T., Wouters, B., Wuite, J., and Team, T. I.: Mass balance of the Greenland Ice Sheet from 1992 to 2018, Nature, 579, 233–239, https://doi.org/10.1038/s41586-019-1855-2, 2020.

Smith, G. C., Allard, R., Babin, M., Bertino, L., Chevallier, M., Corlett, G., Crout, J., Davidson, F., Delille, B., Gille, S. T., Hebert, D., Hyder, P., Intrieri, J., Lagunas, J., Larnicol, G., Kaminski, T., Kater, B., Kauker, F., Marec, C., Mazloff, M., Metzger, E. J., Mordy, C., O'Carroll, A., Olsen, S. M., Phelps, M., Posey, P., Prandi, P., Rehm, E., Reid, P., Rigor, I., Sandven, S., Shupe, M., Swart, S., Smedstad, O. M., Solomon, A., Storto, A., Thibaut, P., Toole, J., Wood, K., Xie, J., Yang, Q., and , t. W. P. S. G.: Polar Ocean Observations: A Critical Gap in the Observing System and Its Effect on Environmental Predictions From Hours to a Season, Frontiers in Marine Science, 6, 429, https://doi.org/10.3389/fmars.2019.00429, https://www.frontiersin.org/article/10.3389/fmars.2019.00429, 2019.

Spada, G.: Glacial Isostatic Adjustment and Contemporary Sea Level Rise: An Overview, Surveys in Geophysics, 38, 153–185, https://doi.org/10.1007/s10712-016-9379-x, https://doi.org/10.1007/s10712-016-9379-x, 2017.

Stammer, D.: Steric and wind-induced changes in TOPEX/POSEIDON large-scale sea surface topography observations, Journal of Geophysical Research: Oceans, 102, 20 987–21 009, https://doi.org/10.1029/97JC01475, https://agupubs.onlinelibrary.wiley.com/doi/abs/10.1029/97JC01475, 1997.

Stammer, D., Ray, R. D., Andersen, O. B., Arbic, B. K., Bosch, W., Carrère, L., Cheng, Y., Chinn, D. S., Dushaw, B. D., Egbert, G. D., Erofeeva, S. Y., Fok, H. S., Green, J. A. M., Griffiths, S., King, M. A., Lapin, V., Lemoine, F. G., Luthcke, S. B., Lyard, F., Morison, J., Müller, M., Padman, L., Richman, J. G., Shriver, J. F., Shum, C. K., Taguchi, E., and Yi, Y.: Accuracy assessment of global barotropic ocean tide models, Reviews of Geophysics, 52, 243–282, https://doi.org/10.1002/2014rg000450, 2014.

van Dam, T., Collilieux, X., Wuite, J., Altamimi, Z., and Ray, J.: Nontidal ocean loading: amplitudes and potential effects in GPS height time series, Journal of Geodesy, 86, 1043–1057, https://doi.org/10.1007/s00190-012-0564-5, https://doi.org/10.1007/s00190-012-0564-5, 2012.

Wang, H., Xiang, L., Jia, L., Jiang, L., Wang, Z., Hu, B., and Gao, P.: Load Love numbers and Green's functions for elastic Earth models PREM, iasp91, ak135, and modified models with refined crustal structure from Crust 2.0, Computers & Geosciences, 49, 190 – 199, https://doi.org/https://doi.org/10.1016/j.cageo.2012.06.022, http://www.sciencedirect.com/science/article/pii/S0098300412002245, 2012.

WCRP, G. S. L. B. G.: Global sea-level budget 1993–present, Earth System Science Data, 10, 1551–1590, https://doi.org/10.5194/essd-10-1551-2018, https://essd.copernicus.org/articles/10/1551/2018/, 2018.

Wiese, D. N., Landerer, F. W., and Watkins, M. M.: Quantifying and reducing leakage errors in the JPL RL05M GRACE mascon solution, Water Resources Research, 52, 7490–7502, https://doi.org/10.1002/2016WR019344, https://agupubs.onlinelibrary.wiley.com/doi/abs/10.1002/2016WR019344, 2016.

Zemp, M., Huss, M., Thibert, E., Eckert, N., McNabb, R., Huber, J., Barandun, M., Machguth, H., Nussbaumer, S. U., Gärtner-Roer, I., Thomson, L., Paul, F., Maussion, F., Kutuzov, S., and Cogley, J. G.: Global glacier mass changes and their contributions to sea-level rise from 1961 to 2016, Nature, 568, 382–386, https://doi.org/10.1038/s41586-019-1071-0, 2019.